In vitro cytotoxic data on Se-methylselenocysteine conjugated to dendritic poly(glycerol) against human squamous carcinoma cells

Nicoli Dolores Gonçalves Correa, Felipe Douglas Silva, Daniel Perez Vieira, Carlos Roberto Jorge Soares & Alvaro Antonio Alencar de Queiroz

Published online: 19 Dec 2021.

Submit your article to this journal ↗

Article views: 74

View related articles ↗

View Crossmark data ↗

Taylor & Francis
Taylor & Francis Group

Check for updates

In vitro cytotoxic data on Se-methylselenocysteine conjugated to dendritic poly(glycerol) against human squamous carcinoma cells

Nicoli Dolores Gonçalves Correa, Felipe Douglas Silva, Daniel Perez Vieira, Carlos Roberto Jorge Soares and Alvaro Antonio Alencar de Queiroz [ID]

Nuclear and Energy Research Institute – IPEN-CNEN, São Paulo, Brazil

ABSTRACT

Polymeric nanoparticles acting as sources of selenium (Se) are currently an interesting topic in cancer chemotherapy. In this study, polyglycerol dendrimer (DPGLy) was functionalized with seleno-methyl-selenocysteine (SeMeCys) by means of Steglich esterification with 4-dimethylaminopyridine/(l-ethyl-3-(3-dimethyl-laminopropyl)carbodiimide) (EDC/DMAP) and cerium chloride as cocatalyst in acetonitrile at quantitative yields of $98 \pm 1\%$. The SeMeCys coupling DPGLy efficiency vs. time were determined by Fourier Transform infrared spectroscopy (FTIR) and ultraviolet–visible (UV–Vis) spectroscopy. The cytotoxic effects of SeMeCys–DPGLy on the Chinese Hamster ovary cell line (CHO-K1) and head and neck squamous cell carcinoma (HNSCC) cells line were assessed by MTS (3-(4,5-dimethylthiazol-2-yl)-5-(3-carboxy-methoxyphenyl)-2-(4-sulfophenyl)-2H-tetrazolium) assay. No signs of general toxicity of SeMeCys–DPGLy against CHO-K1 cells were detectable at which cell viability was greater than 98%. MTS assays revealed that SeMeCys–DPGLy reduced HNSCC cell viability and proliferation at higher doses and long incubation times.

1. Introduction

Selenium (Se) is found in a variety of organic molecules such as selenoaminoacids, selenopeptides and selenoproteins with interesting therapeutic properties [1–3]. Organoselenium (OSe) compounds have aroused substantial attention for their anti-cancer potential and inflammation regulation [4–10].

Although the mechanistic bases of selenium toxicity are still not fully understood, the anticancer property of OSe compounds is generally attributed to their ability to the induction of mitochondria-mediated apoptosis of cancer cells triggering excessive production of reactive oxygen species (ROS) inducing apoptosis by activating the mitogen-activated protein kinase (MAPK) and p53 signaling pathways [11,12].

However, the exact molecular role played by OSe in the mechanisms of carcinogenesis is still elusive.

Despite the great promise that OSe offers for cancer therapy, their aromatic nature [13] contributes to their high lattice energy for their dissolution and the inability of the OSe molecules to form hydrogen bonds with water. The lack of good aqueous solubility limits the clinical use of OSe compounds [14–16].

Several approaches have been employed to enhance the solubility of OSe compounds, including nanosizing [17], stimuli-responsive copolymers [18], formation of inclusion complexes [19] or coordination with dendrimers [20]. In this context, dendritic polyglycerol (DPGLy) has been proven to be one of the most effective when trying to increase aqueous solubility of the poor and sparingly soluble drugs which results in increased bioavailability of anticancer drugs [21].

The potential applications of DPGLy to cancer treatment are broadened by their ability to increase the water-solubility of poorly soluble drugs through the hydrotropy mechanism [22]. To date, DPGLy has been used for either non-covalently encapsulation of anticancer drug in their core or covalently conjugated to its surface [23–28].

The present study describes the synthesis of DPGLy conjugated with Se-methylselenocysteine (SeMeCys), designed to be considered as a non-cytotoxic nanocarrier for SeMeCys. SeMeCys is a chemopreventive agent that blocks the cell cycle progression and proliferation of premalignant mammary lesions and induces apoptosis of cancer cell lines [29]. These effects can be attributed to mitochondrial dysfunction induced by ROS generation and by activation of Bax–Bak proteins [30]. The Bax–Bak proteins are capable of perforating the mitochondrial outer membrane to mediate cell death by apoptosis.

The poor solubility of SeMeCys in physiological medium (pH 7.2) indicates that this compound will not bioaccumulate in mitochondrial membrane of tumoral cells compromising your efficiency in cancer treatment. To overcome this limitation and to enhance the accumulation of SeMeCys in solid tumors *via* the enhanced permeability and retention (EPR) SeMeCys was esterified with DPGLy. The amphiphilic property of DPGLy facilitates the micelle formation which could play an important function in the process of intracellular uptake and bioaccumulation by tumor cells.

The objective of this *in vitro* study was to quantify the relative cytotoxic effect of the conjugate SeMeCys–DPGLy on head and neck squamous cell carcinoma (HNSCC) SCC9 cells line, using Chinese hamster ovary cell (CHO-K1) cells as a control for comparison. The growing statistics of new HNSCC cases and annual deaths have worried health authorities around the world [31]. A recent study demonstrates that the Ose compound methylseleninic acid (MSA) induces significant lipid peroxidation and radiation sensitivity in HNSCC cells line [32].

In this work, we report the synthesis, characterization and *in vitro* cytotoxicity of the conjugate SeMeCys–DPGLy against HNSCC cells at concentrations ranging from 0.01 to 1000 $\mu g\,mL^{-1}$. The physicochemical properties of the prepared SeMeCys–DPGLy were characterized by the spectroscopic techniques Matrix Assisted Laser Desorption Ionization – Time of Flight (Maldi-Tof), attenuated total reflection with Fourier transform infrared (ATR-FTIR) and ultraviolet–visible (UV–Vis). The cytotoxicity results provide evidence that SeMeCys–DPGLy is a perspective candidate for further *in vivo* assays.

2. Experimental section

2.1. Materials

All chemicals are commercially available (Sigma-Aldrich, São Paulo-Brazil) and were used as received: glycerol (1,2,3-propenotriol, purity ≥99,5%), allyl bromide (3-bromo-1-propene, purity ≥97%), N,N-dimethylformamide (DMF, anhydrous, purity 99.8%), potassium hydroxide (KOH, purity 90%), 4-methylmorpholine N-oxide (NMO, purity 97%), osmium tetroxide (OsO_4, purity 99.8%), Se-methylselenocysteine hydrochloride (purity ≥95%, SeMeCys), N-(3-dimethylaminopropyl)-N'-ethylcarbodiimide hydrochloride (EDC.HCl, 98%), N,N-dimethylaminopyridine (DMAP, purity 98%). All solvents used were purchased from Sigma-Aldrich with 98.5% purity (minimum) and with no previous treatment.

2.2. General procedure for the synthesis and characterization of SeMeCys–DPGLy

DPGly with generation 3 was synthesized through a two-step process based on allylation and catalytic dihydroxylation steps starting from the deprotonated glycerol as core unit in according to previously reported methods [33]. One of the motivations that have driven the use of DPGLy with generation 3 (DPGLy G3) is their octanol/water partition coefficient would indicate that they are not lipophilic and this to be easily cleared from the blood through the kidneys and eliminates the need for biodegradability [34]. Additionally, the literature demonstrates that lower-generation dendrimers are preferred over those of higher generations as these are less cytotoxic, less immunogenic and more biocompatible [35]. The DPGLy G3 with an average of 24 hydroxyls per molecule was synthesized and their real mass determined from Maldi-Tof (Bruker Microflex LT MALDI-TOF MS, Germany) was found to be 1.6–1.7 kDa [36,37]. This value was consistent with the theoretical molecular weight of PGLD G3 (1.690 kDa) previously reported [38]. The successful synthesis of PGLD G3 (88% yield) was confirmed by ^1H NMR and ^{13}C NMR spectroscopy. ^1H NMR (500 MHz, Bruker Avance, D_2O, 298 K), δ (ppm): 3.76–3.49 (88H, m); 3.79 (l0H, m); 3.89 (12H, m). ^{13}C NMR (400 MHz, Varian Inova, D_2O, 298 K), δ (ppm): 69.4, 70.3–70.5, 72.2 (CH_2O); 78.2, 77.0 (CHO); 60.8–61.1 (CH_2OH); 68.8, 70.5 (CHOH). ATR-FTIR (film under diamond crystal): 1090 cm^{-1} (ν_{CO}, ether), 2860–2928 cm^{-1} (ν_{CH} and ν_{CH2}, aliphatic chain), 3380 cm^{-1} (ν_{OH}).

The amine group of SeMeCys was previously protected with the *tert*-butyloxycarbonyl (Boc) groups to avoid secondary reactions. Protection of the SeMeCys amine group was accomplished in acetonitrile solution using DMAP [39]. The direct esterification of Boc–SeMeCys with DPGLy was carried out through Steglich esterification employing $CeCl_3$ as a highly effective cocatalyst providing SeMeCys–DPGLy esters in excellent yields [40]. Because cerium is relatively nontoxic, easy to handle, low cost and recoverable in water their use in esterification of SeMeCys with DPGLy appears to be more safe and green method to synthesis of sustainable biomaterials and drugs for oncology. The exact mechanism of action of $CeCl_3$ in this work is still unknown, but it seems to involve a complexation with the peripheral hydroxyl groups of
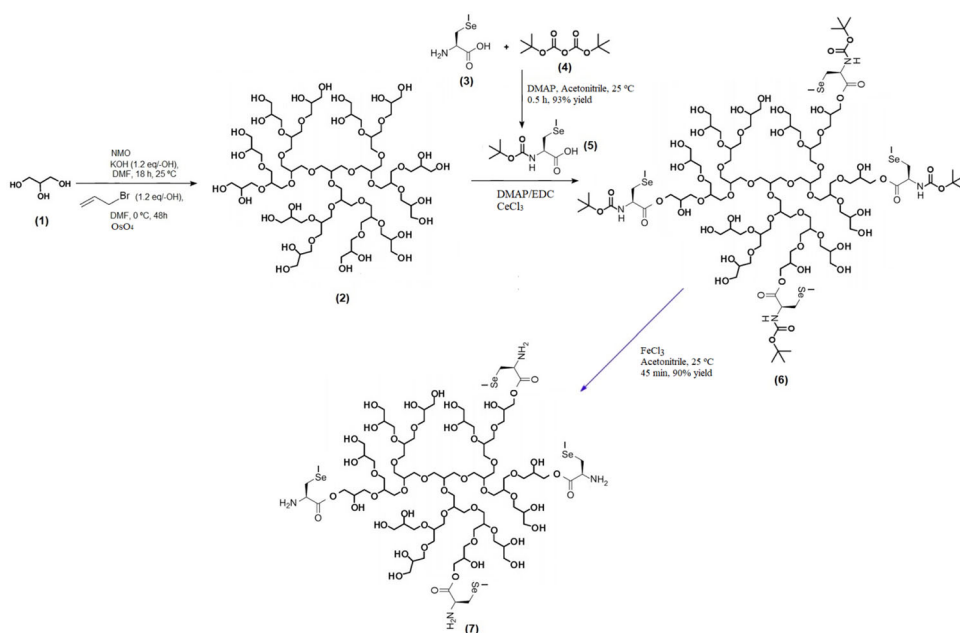
Figure 1. Illustration of the chemical synthesis of SeMeCys–DPGLy (7). Reagents and conditions: allylation of the hydroxyl group of glycerol (1) using allyl bromide resulting DPGLy (2); t-Boc protection of amino groups of SeMeCys (3) to form Boc–SeMeCys–DPGLy (5), esterification reaction of (2) with (5) in DMAP/EDC and CeCl$_3$ as cocatalyst resulting Boc–SeMeCys–DPGLy ester (6) and deprotection of t-Boc resulting the ester SeMeCys–DPGLy (7).

DPGLy increasing its nucleophilicity due to electronic delocalization of charge of peripheral hydroxyl groups. The esterification of DPGLy was accomplished by coupling the hydroxyl functionalities of DPGLy with the carboxy termini of Boc–SeMeCys. Then, EDC·HCl was used as a condensation agent, 4-(dimethylamino)pyridine (DMAP) as a base, CeCl$_3$ as cocatalyst and acetonitrile as a solvent.

The coupling the Boc–SeMeCys to DPGLy, was carried out in a 200 mL one-necked flask equipped with a stopper and a magnetic stirring bar. DPGLy (0.5 mmol) and CeCl$_3$·7H$_2$O (0.1 mmol) was added into the flask and dissolved in acetonitrile (30 mL) at room temperature (25 °C). DMAP (0.632 mmol) was introduced, followed by the addition of Boc–SeMeCys (6.34 mmol) and EDC·HCl (6.32 mmol). After stirring for 60 min at room temperature (25 °C), the solvent was evaporated under reduced pressure. The cleavage of t-Boc groups on SeMeCys has been carried out successfully in acetonitrile at room temperature (25 °C) using FeCl$_3$ (1 mmol) as catalyst at yield of 90% [41]. The resultant SeMeCys–DPGLy was then re-dissolved in deionized water (DI) and placed in 1 kDa cutoff dialysis tubing in a 1 L beaker filled with DI water. The SeMeCys–DPGLy was trapped inside, while the lighter precursor materials could diffuse out of the bag into the surrounding fluid (dialyte). The DI water in the 1 L beaker was replaced after 2, 4, 8, 16, 24 and 48 h. After dialysis purification, the SeMeCys–DPGLy was lyophilized. The purified product SeMeCys–DPGLy was obtained as a yellow liquid with a high viscosity with 98% of yield after lyophilization. Figure 1 illustrates the general procedure to synthesis of SeMeCys–DPGLy.

ATR-FTIR spectroscopy was used for monitoring the synthesis of SeMeCys–DPGLy (7). ATR-FTIR spectra of DPGLy (2) and SeMeCys–DPGLy (7) were collected by using a Shimadzu, IRTracer 100 Fourier Transform Infrared Spectrometer equipped with a MIRacle diamond Attenuated Total Reflection-ATR crystal. The spectra were recorded in the 500–4000 cm^{-1} range with a lateral resolution of 2 cm^{-1} and 200 scans.

The purity and structure of SeMeCys–DPGLy (7) was confirmed by Maldi-Tof spectroscopy. The DPGLy (2) and SeMeCys–DPGLy (7) solutions concentration was 5 $mg\,mL^{-1}$ aqueous acetone (acetone/water, 70:30, v/v). A matrix solution of dihydroxybenzoic acid (DHB, 50 $mg\,mL^{-1}$) in acetone was prepared. The analyzed mixture of DPGLy (2) or SeMeCys-DPGLy (7) is a matrix containing 1:4 (v/v) of the sample and the DHB solutions, respectively. An aliquot of the mixture was applied to the sample probe and the solvent was evaporated. Mass spectra were acquired in the reflector positive mode on a Bruker MicroFlex LT MALDI-TOF MS.

The aqueous solubility of DPGLy (2) and SeMeCys–DPGLy (7) was determined using the octanol/water partition coefficient (log P). The log P of DPGLy (2) and SeMeCys–DPGLy (7) in octanol/water byphasic system were obtained using phosphate buffered saline solution (PBS) pH 7.4 at 37 °C. A saturated n-octanol buffer solution containing 200 μg/mL of DPGLy (2) or 200 μg/mL of SeMeCys-DPGLy (7) and the n-octanol saturated PBS pH 7.4 in equal proportions was mixed in a 5 mL vial glass container. The container was placed into a water bath shaker at 37 ± 0.5 °C and shaken at two hundred times per min until equilibrium was attained between the DPGLy (2) or SeMeCys–DPGLy (7) concentrations in the PBS and in the oil phase. After that, the aqueous phase of the solution was separated from the n-octanol oil phase by centrifugation at 3000 rpm for 10 min. Each phase was analyzed for its content of DPGLy (2) or SeMeCys–DPGLy (7) by UV–Vis spectrophotometer method (Cary 50). The log P of DPGLy (2) and SeMeCys–DPGLy (7) in the aqueous two-phase systems was defined as the following equation [42]:

$$\log P = \log \frac{C_{oct}}{C_w} \tag{1}$$

where C_{oct} and C_w are DPGLy (2) (or SeMeCys–DPGLy (7)) saturation concentration in octanol and water, respectively.

The mean log P value of DPGLy (2) and SeMeCys–DPGLy (7) from three measurements were analyzed by one-way ANOVA statistic ($p < .05$) and expressed as mean value ± standard deviation.

The quantitative analysis of SeMeCys (3) coupled to DPGLy (2) was performed using UV–VIS spectrophotometry (Varian, Cary 50). The procedure is based on complex formation of 4,5-diamino-6-hydroxy-2-mercapto pyrimidine (DAHMP, Sigma-Aldrich) with Se (IV) ions in the presence of sodium dodecyl sulfate (SDS) [43]. SeMeCys–DPGLy (7) was decomposed in a microwave oven by acid digestion using 10 mL of HCL 3 $mol\,L^{-1}$ and heating at 150 °C for 30 min for reduction of Se(VI) to Se(IV). Then, 10 mL of the neutralized digested sample was added to 50 mL measuring flask followed by the addition of 3.0 mL of citric acid 0.1 $mol\,L^{-1}$ and 1.50 mL of

DAHMP 20 mmol L^{-1}. After extraction of the complex by SDS, the absorbance was measured at 458 nm in a quartz cell versus a blank.

2.3. In vitro biological assays

2.3.1. In vitro cytotoxic evaluation of SeMeCys–DPGLy

CHO-K1 (CCL-61) and HNSCC (SCC 9, CRL-1629) were purchased from American Type Culture Collection (ATCC). According to ATCC protocols, CHO-K1 and SCC-9 cells were cultured in Dulbecco's Modified Eagle's medium (DMEM, Gibco, NY-EUA) /F10 nutrient mixture (1:1, v/v) supplemented with 10% Fetal Bovine Serum (FBS, Gibco), 1% L-glutamine (Thermo Fisher, SP-Brazil), 1% sodium pyruvate (Thermo Fisher) and 1% penicillin/streptomycin (Thermo Fisher) solutions. The CHO-K1 and SCC9 cells lines were incubated at 37 °C in a humidified atmosphere of 95% air and 5% of carbon dioxide (CO_2).

The effect of SeMeCys (3) and SeMeCys–DPGLy (7) on viability of CHO-K1 and SCC 9 cells was determined by the 3-(4,5-dimethylthiazol-2-yl)-5-(3-carboxymethoxy-phenyl)-2-(4-sulfophenyl)-2H-tetrazolium (MTS) in the presence of phenazine methosulfate (PMS) colorimetric assay, as described previously [44]. MTS is bioreduced by NADPH-dependent dehydrogenase enzymes in metabolically active cells and the formazan dye produced is soluble in culture media (CM). Briefly, 2.5×10^5 cells/well in 96-well plates were treated with different concentrations of SeMeCys (3) or SeMeCys–DPGLy (7) (0, 0.01, 0.1, 1, 10, 100 or 1000 μg mL^{-1}) and incubated at 37 °C for 24, 48 or 96 h in a humidified 5% CO_2 incubator (Thermo Fisher Scientific, SP-Brasil). At the appropriate time, the CM with different concentrations of SeMeCys (3) or SeMeCys–DPGly (7) was pipetted and replaced with 100 μL/well of a 5:1 volume ratio mixture of respective media and the freshly prepared MTS/PMS (20:1) assay solution (3.6 mM in Dulbeccós phosphate buffered saline, DPBS, pH 7.4) and incubated for 2 h at 37 °C in a humidified 5% CO_2 incubator. Afterward, the absorbance was measured at 490 nm in a microplate reader (MR4000, Dynatech). Untreated CHO-K1 and SCC9 cells were also run under identical conditions and served as control. A positive control of 0.5% (w/v) phenol in 0.9% (w/v) saline solution was incorporated in the experiment. The viability of CHO-K1 and SCC9 cells cultured in the presence of the SeMeCys (3) or SeMeCys–DPGLy (7) was calculated as a percentage of control cells.

The surviving fraction of cells was calculated for each assay as the percentage of cell viability, CV (%):

$$CV\ (\%) = \frac{OD_{ts}}{OD_{cs}} \cdot 100 \qquad (2)$$

where OD_{ts} is the optical density of test sample and OD_{cs} is the optical density of the control sample.

2.3.2. Apoptosis assay

The apoptosis induced by treatment with SeMeCys–DPGly (7) was studied after dyeing SCC9 cells with a fluorescent mixture of acridine orange (AO) and ethidium bromide (AO/EtBr) in according to literature [45]. The viable cells stain uniformly,

whereas cells in early apoptotic stage stains bright green color. Moreover, in the presence of EtBr late apoptotic cells stains orange to red in color [46]. SCC9 cells were seeded in 96-well plates (2.5×10^5 cells/well), incubated for 24 h for adherence followed by incubation with or without SeMeCys–DPGLy (7) at a concentration of $1000\,\mu\mathrm{g\,mL}^{-1}$ for 72 h at $37\,^{\circ}\mathrm{C}$ in 5% CO_2 incubator. The cells were washed with phosphate buffer saline (PBS, pH 7.4), added $10\,\mu\mathrm{L}$ of AO and EtBr ($100\,\mu\mathrm{g\,mL}^{-1}$, Sigma-Aldrich) respectively to each well, and incubated for 15 min in CO_2 incubator. Following incubation, the medium was aspirated, and washed with PBS. Apoptosis was assessed by identifying apoptotic, viable and nonviable cells under a fluorescent microscope (Nikon) with a blue excitation (480 nm) and a barrier filter of 515–530 nm. Quantitative measures of apoptosis were obtained with ImageJ software (version 1.49, http://imagej.nih.gov/ij/; provided in the public domain by the National Institutes of Health, Bethesda, MD, USA). The images scripts were coded using IJ1 programming language on Fiji image processing software (http://fiji.sc/Fiji, in the public domain). The results were expressed as apoptosis index (AI) in according to Equation (3):

$$\mathrm{AI}\ (\%) = \frac{\mathrm{IA} + \mathrm{LA}}{\sum C}.100 \tag{3}$$

where IA is the number of cells in initial apoptosis, LA is the number of cells in late apoptosis and $\sum C$ is the total number of cells.

2.4. Statistics

Every experiment was replicated three times and data sets were expressed as means ± standard deviations (SD). Statistical significance was determined by the unpaired one-way ANOVA or t test at the 95% significance level ($p < .05$).

3. Results and discussion

3.1. Synthesis and characterization

Typical ATR-FTIR spectra of compounds DPGLy (2), Boc-SeMeCys (5) and Boc-SeMeCys–DPGLy (6) recorded at room temperature ($25\,^{\circ}\mathrm{C}$) are presented in Figure 2. The absorption peak at $1690\,\mathrm{cm}^{-1}$ (Figure 2(a)) was attributed to amide vibrations ($\nu\mathrm{CO–NH}$) indicating the protection of amine group of SeMeCys (3) by t-butoxycarbonyl. The peaks around 1360 and $1390\,\mathrm{cm}^{-1}$ (Figure 2(a)) belong to the Boc group were also characteristic of the formation of Boc–SeMeCys (5). FTIR spectra of DPGLy (2) (Figure 2(b)) displayed bands in the region from 3450, 2940–2900 and $1200\,\mathrm{cm}^{-1}$ characteristics of the stretching vibrations of hydroxyl groups ($\nu\mathrm{OH}$), antisymmetric and symmetric stretching of the methylene groups ($\nu_{as}\,CH_2$, $\nu_s\,CH_2$) and stretching vibrations of ether bonds (C–O–C) of DPGLy (2) (Figure 2(b)), respectively. These results are in good agreement with literature [47].

The band that appears at about $1750\,\mathrm{cm}^{-1}$ in Boc–SeMeCys–DPGLy (7) (Figure 2(b, c)) can been assigned to C$=$O stretching vibration of Boc–SeMeCys (3)
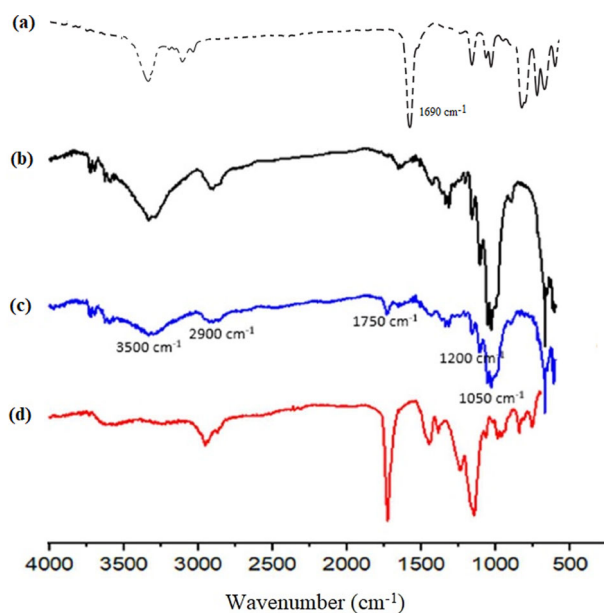
Figure 2. ATR-FTIR spectra measured at room temperature (25 °C) of: Boc–SeMeCys (5) (a), DPGLy (2) (b) and Boc–SeMeCys–DPGLy (6) after 5 min (c) and 30 min (d) of esterification reaction, respectively. For quantitative analysis of the esterification process the Boc–SeMeCys (5) (a) spectrum was subtracted from the Boc–SeMeCys–DPGLy (6) spectra (c, d).

esterified carboxylic group and represent a clear differential feature between the spectra of Boc–SeMeCys (5) and DPGLy (2). Moreover, the Boc–SeMeCys–DPGLy (7) spectrum (Figure 2(b, c)) shows significantly reduced hydroxyl band and the band at $2900 \, cm^{-1}$ correspondent to stretching of methyl groups (CH_3) of Boc–SeMeCys (3) increased, confirming consumption of hydroxyl groups of DPGLy (2) during esterification process (Figure 2(b, c)).

The increase in the intensity of carbonyl absorption band assigned at $1750 \, cm^{-1}$ was used to monitor the ester conversion during the esterification reaction between Boc–SeMeCys (5) and DPGLy (2). Quantification is based on the Beer–Lambert law and the conversion degree (p) was calculated as the ratio between the absorbance of the ester group and that of an internal standard, a group whose concentration does not change during the esterification reaction course:

$$p = 1 - \left[\frac{\left(\frac{A_{C=O}}{A_{CH2}} \right)_{t=t'}}{\left(\frac{A_{C=O}}{A_{CH2}} \right)_{t=o}} \right] \tag{4}$$

where A = area of absorption band of ester groups (C=O) of SeMeCys–DPGLy (7) and methylene (CH_2) groups of the DPGLy (2) at initial ($t=0$) and reaction time ($t=t'$), respectively. $A = -\log T$.

In this study, the absorbance corresponding to the CH_2 stretching region, assigned at approximately $2900 \, cm^{-1}$, was used. Figure 3 shows the data extracted from the FTIR experiment and the corresponding calculated ester conversion curve. All the
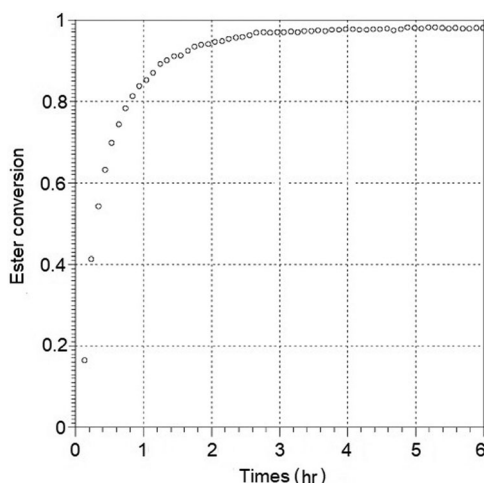
Figure 3. Ester conversion during the esterification reaction between Boc–SeMeCys (5) and DPGLy (2) using DMAP/EDC and CeCl$_3$ as cocatalyst at room temperature (25 °C).

experiments were done in triplicate. The conversion (p) achieved after 3 h of reaction was around 98% of ester (Figure 3). This value corresponds to about eleven primary hydroxyls of DPGLy (2) esterified by SeMeCys (3).

The Se content coupled to DPGLy (2) in SeMeCys–DPGLy (7) conjugate was determined by UV–Vis after reduction of Se(VI) to Se(IV) in microwave. Figure 4 shows the UV–Vis absorption spectra of the complex formed between DAHMP and Se(IV) from digested SeMeCys–DPGLy (7). The UV–Vis spectrum exhibits an absorption maximum at 458 nm, due to the formation of charge transfer of the type ligand (π) $\rightarrow$ $^1B_{1g}$ (SeIV) and ligand (σ) $\rightarrow$ $^1B_{1g}$ (SeIV), respectively, in a typically distorted square–planar environment around the metal ion [48]. The amount of SeMeCys (3) coupled to DPGLy (2) reached a maximum of 10 mg per g of dendrimer after 3 h (Figure 4) which corresponded to almost all of the primary hydroxyl groups in the dendrimer in good agreement with the ATR-FTIR data (Figure 3).

The MALDI-TOF mass spectra of DPGLy (2) and SeMeCys–DPGLy (7) are presented in Figure 5(a) and (b), respectively. The MALDI-TOF spectrum of DPGLy (2) (Figure 5(a)) exhibits a single peak at the m/z around 1650 indicating the existence of glycerol core with 17 monomeric units. The higher $[M + H]^+$ peak of SeMeCys–DPGLy (7) is 3646 (Figure 5(b)). Since the molecular weight of DPGLy (2) is 1650, the difference is 1996. This difference corresponds to 11 molecules of SeMeCys (3) combined with DPGLy (2) and excludes the possible existence of noncovalent conjugates in the sample.

The variations of log P of the DPGLy (2) as a function of the number of primary hydroxyls of dendrimer replaced by SeMeCys (3) are reported in Figure 6. Among the partition coefficients, the DPGLy (2) had the lowest log P value (-7.96 ± 0.45) and DPGLy (2) with higher number of hydroxyl groups substituted by SeMeCys (3), that is, with 11 primary substituted hydroxyl groups had the greatest log P (-2.13 ± 0.12). On the other hand, an increase in substitution of primary hydroxyls groups of DPGLy (2) by SeMeCys (3) will increase significantly the log P value of the dendrimer. This effect presumably arises from a weakening of the hydrogen bonding
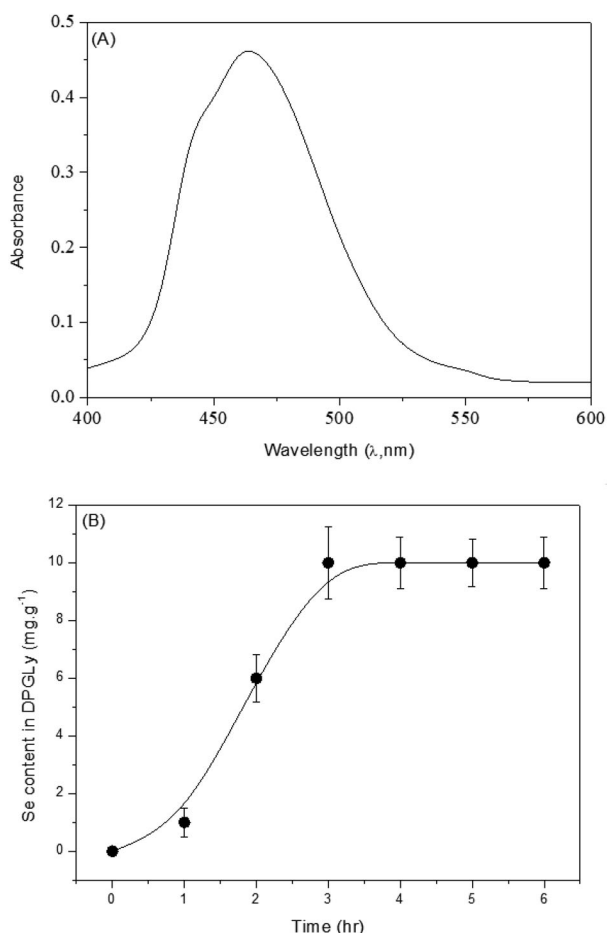
Figure 4. UV–Vis spectrum of Se(IV):DAHMP complex (A) and Se content in the SeMeCys–DPGLy (7) (B). The calibration curve obeys the equation $A = 0.04018.C$ (mg/mL^{-1}) $+ 0.0175$, which has a good Pearson coefficient ($r^2 = 0.9984$) over a wide concentration range of Se at the interval of 1–12 mg/mL^{-1}.

in water of the DPGLy (2) by the SeMeCys (3) substituents. The increase in log P value for the highest substitution of primary hydroxyls groups of DPGLy (2) by SeMeCys (3) would indicate that the conjugate has its amphiphilic character shifted to lipophilicity. This increase in lipohilicity may contribute to its permeability promoting their bioaccumulation in the tumoral cells. Moreover, the non-esterified secondary hydroxyls groups of DPGLy (2) may still act as hydrotropic sites for solubilizing the SeMeCys–DPGLy (7) conjugate in water.

3.2. Biological section

3.2.1. Cytotoxicity analysis

To assess the cytotoxicity against CHO-K1 cells the cell viability on control substrate and on SeMeCys·HCl (3) and SeMeCys–DPGly (7) were determined using the MTS
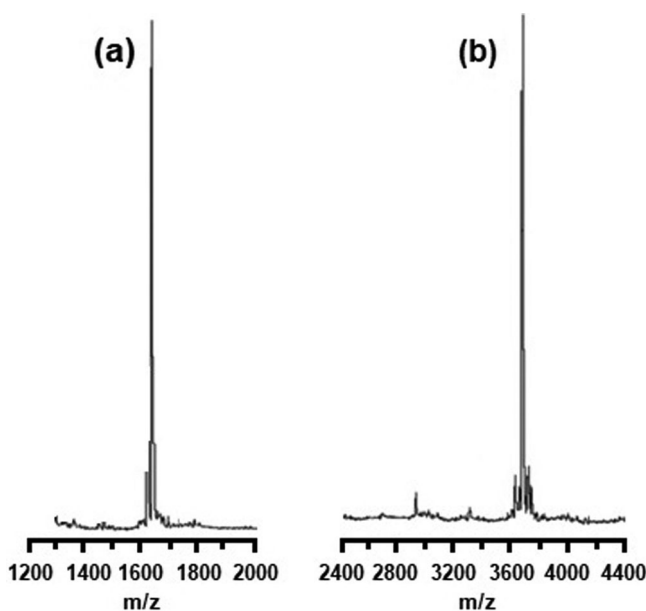
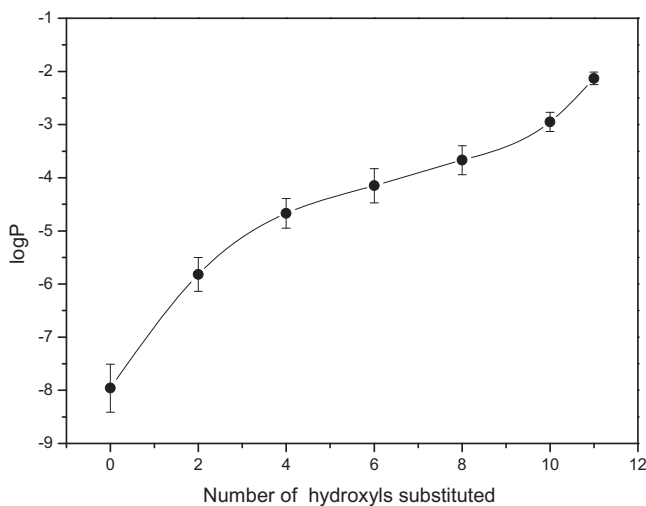Figure 5. MALDI mass spectra of DPGLy (2) (a) and their conjugate SeMeCys–DPGLy (7) (b).

Figure 6. Dependence of the octanol/water partition coefficients (log P) on the number of primary hydroxyls of DPGLy (2) replaced by SeMeCys (3).

assay after 24, 48 and 72 h of incubation and the results are shown in Figure 7(a, b). The MTS assay showed that the optical density of SeMeCys·HCl (3) was not statistically significantly different from that of the negative control after 24, 48 or 72 h of culture even when treated at SeMeCys·HCl (3) concentrations as high as $1000 \, \mu g \, mL^{-1}$ ($p > .05$; Figure 7(a)). The MTS assays indicated that CHO-K1 cells had normal mitochondrial function in presence of SeMeCys·HCl (3) as on the negative control substrate, pointing out that the selenium aminoacid (3) did not affect cell viability or proliferation.
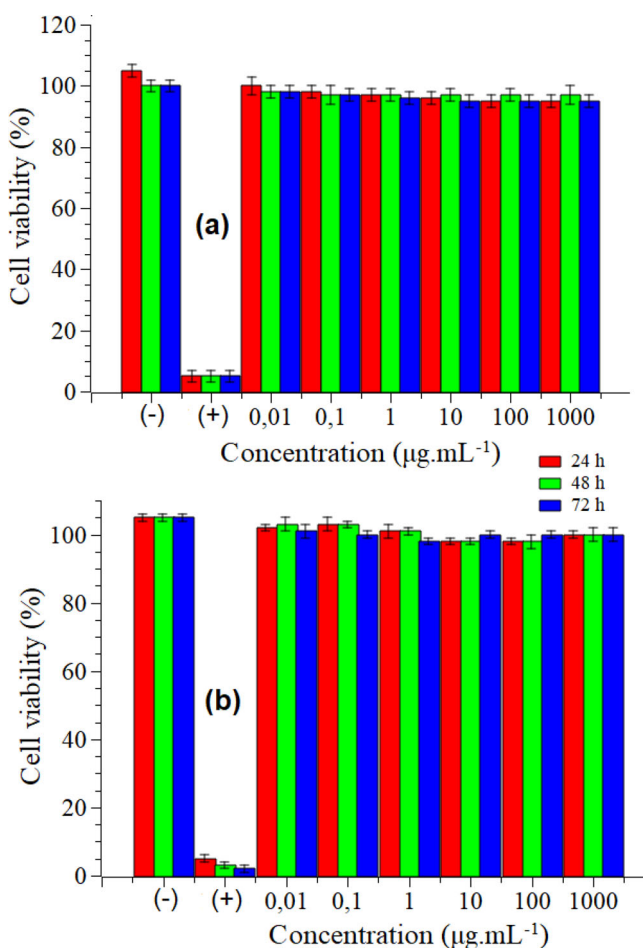
Figure 7. Cell viability measured by CHO-K1 after SeMeCys (3) (a) and SeMeCys–DPGLy (7) (b) treatment with different concentrations after 24, 48 and 72 h of incubation. (−): negative control (culture medium), (+): positive control (phenol 0.5% w/v). Data are represented by mean $\pm$ standard deviation ($n = 3$).

According to the cytotoxicity test results in Figure 7(b), the conjugate SeMeCys–DPGly (7) also preserves the mitochondrial function of CHO-K1 cells. The MTS assay showed that the cell viability of CHO-K1 cells cultured with the negative control and with SeMeCys–DPGLy (7) was not significantly different from that of the control after exposure times as high as 72 h of culture ($p > .05$). As expected, cell viability in the positive control was lower than that of the negative control and the SeMeCys–DPGLy (7) ($p < .01$) (Figure 7(b)), which shows that cells cultured in the positive control did not survive to the application of the phenol 0.5%. The percentage of CHO-K1 viability on SeMeCys–DPGLy (7) was similar to that observed on the negative control after 72 h of culture ($p > .05$), revealing that cell activity was not influenced by the presence of SeMeCys–DPGLy (7). This finding confirms that the conjugate SeMeCys–DPGLy (7) exhibits good biocompatibility against CHO-K1 cells.
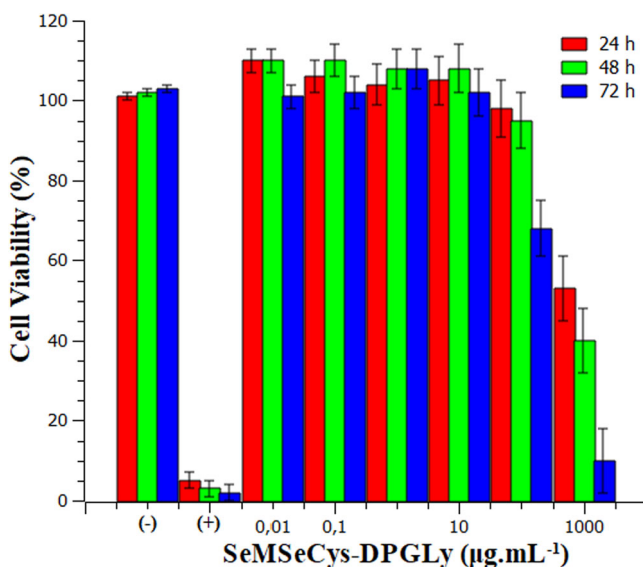
Figure 8. *In vitro* activity of SeMeCys–DPGLy (7) against the HNSCC cell line SCC9, relative to untreated cells at 24, 48 and 72 h. (−): negative control (culture medium), (+): positive control (phenol 0.5% w/v). Data are represented by mean $\pm$ standard deviation ($n = 3$).
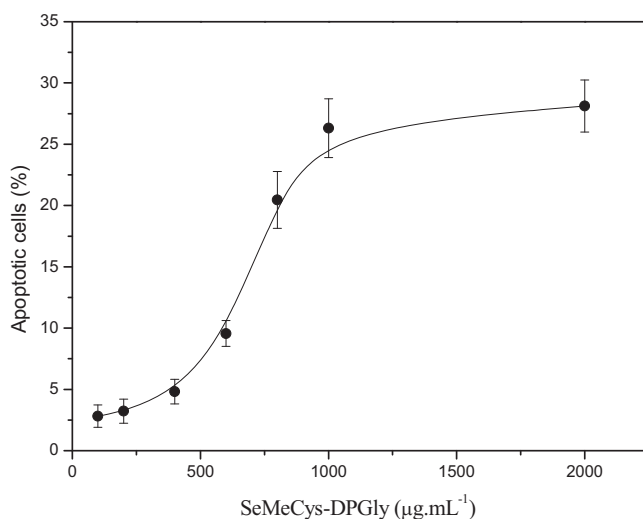

Figure 9. Percentage of apoptotic cells induced by SeMeCys–DPGLy (7) identified using AO/EtBr method after 72 h of incubation time. Data are presented as mean $\pm$ SD ($n = 3$).

3.2.2. In vitro effect of SeMeCys–DPGLy on SCC9 cells

The *in vitro* effect of SeMeCys–DPGLy (7) against SCC9 cells is shown in Figure 8. The results indicated that SeMeCys–DPGLy (7) inhibited the growth of the SCC9 cells which was dependent on both dosage and exposure time (Figure 8). For exposure times as high as 72 h, cell viability remained relatively high except at the maximum dosage of 100 μg SeMeCys–DPGLy (7)/mL media, where the cell viability reduces to 65%. However, at 1000 μg/mL media, SeMeCys–DPGLy (7) began to

induce a significantly cytotoxic effect against SCC9 cells. A possible explanation for the activity of the SeMeCys–DPGLy (7) against SCC9 cells may be due to the release of apoptogenic factors caused by the disruption of the mitochondrial cellular membrane [49,50]. However, further research will be needed to determine if this mechanism is plausible for the SeMeCys–DPGLy (7).

The primary mechanism by which chemotherapeutics destroy tumor cells is by inducing apoptosis. High levels of apoptosis in cancer cells are strongly associated with chemotherapeutic sensitivity [50]. The efficacy of SeMeCys–DPGLy (7) should be measured by their ability to promote the apoptosis of SCC9 cells. Figure 9 suggests that the treatment of SCC9 cells with $1000\,\mu g\,mL^{-1}$ or more induced apoptosis in about 26% of SCC9 cells.

4. Conclusions

In the current study, SeMeCys–DPGLy (7) were successfully synthesized, characterized and used in cell viability tests on CHO-K1 and SCC9 cell lines. The cytotoxicity experiments indicate that SeMeCys–DPGLy (7) possesses good biocompatibility and appears does not affect the mitochondrial function and proliferation of CHO-K1 cells. The *in vitro* results indicated that SeMeCys–DPGLy (7) have their greatest cytotoxic effect against SCC9 cells line when present in the cells for 72 h at concentrations of at least $1000\,\mu g/mL$ exhibiting dose response dependence. Despite the biological promising effects of SeMeCys–DPGLy (7) against SCC9 cells, little is known about their actuation mechanism in the cells line studied. Further studies may elucidate the mechanisms involved in the cytotoxic behavior of the SeMeCys–DPGLy (7) against SCC9 cells evaluated in the present work. These studies will open up new possibilities for understanding and validating SeMeCys–DPGLy (7) as an alternative therapeutic agent against SCC9 cells. In a next step, the exact mechanism of SCC9 apoptosis in the exponential and stationary phases of growth will be studied. The exact knowledge of the apoptosis induction process of SCC9 cells may offer promising perspectives for the use of SeMeCys–DPGly (7) and should be the object of future studies.

Disclosure statement

Funding

ORCID

Alvaro Antonio Alencar de Queiroz 🆔 http://orcid.org/0000-0002-1769-7022

References

[1]   Marshall JR, Ip C, Romano K, et al. Methyl selenocysteine: single-dose pharmacokinetics in men. Cancer Prev Res (Phila). 2011;4(11):1938–1944.
[2]   Tran P, Kopel J, Fralick JA, et al. The use of an organo-selenium peptide to develop new antimicrobials that target a specific bacteria. Antibiotics. 2021;10(6):611–617.
[3]   Mangiapane E, Pessione A, Pessione E. Selenium and selenoproteins: an overview on different biological systems. Curr Protein Pept Sci. 2014;15(4):1–9.
[4]   Gandin V, Khalkar P, Braude J, et al. Organic selenium compounds as potential chemotherapeutic agents for improved cancer treatment. Free Radic Biol Med. 2018;127: 80–97.
[5]   Sanmartin C, Plano D, Sharma AK, et al. Selenium compounds, apoptosis and other types of cell death: an overview for cancer therapy. Int J Mol Sci. 2012;13(8):9649–9672.
[6]   Hariharan S, Dharmaraj S. Selenium and selenoproteins: it's role in regulation of inflammation. Inflammopharmacology. 2020;28(3):667–695.
[7]   Spengler G, Gajdács M, Marc MA, et al. Organoselenium compounds as novel adjuvants of chemotherapy drugs – a promising approach to fight cancer drug resistance. Molecules. 2019;24(2):336.
[8]   Tan HW, Mo HY, Lau ATY, et al. Selenium species: current status and potentials in cancer prevention and therapy. Int J Mol Sci. 2019;20:1–26.
[9]   Fernandes AP, Gandin V. Selenium compounds as therapeutic agents in cancer. Biochim Biophys Acta. 2015;1850(8):1642–1660.
[10]   Radomska D, Czarnomysy R, Radomski D, et al. Selenium compounds as novel potential anticancer agents. Int J Mol Sci. 2021;22:1–27.
[11]   Chen Z, Lai H, Hou L, et al. Rational design and action mechanisms of chemically innovative organoselenium in cancer therapy. Chem Commun (Camb). 2019;56(2): 179–196.
[12]   Smith ML, Lancia JK, Mercer TI, et al. Selenium compounds regulate p53 by common and distinctive mechanisms. Anticancer Res. 2004;24(3A):1401–1408.
[13]   Jain VK. An overview of organoselenium chemistry: from fundamentals to synthesis. In: Jain VK, Priyadarsini KI, editors. Organoselenium compounds in biology and medicine: synthesis, biological and therapeutic treatments. London (UK): The Royal Society of Chemistry; 2018. p. 1–33.
[14]   Nogueira CW, Barbosa NV, Rocha JBT. Toxicology and pharmacology of synthetic organoselenium compounds: an update. Arch Toxicol. 2021;95(4):1179–1226.
[15]   Prigol M, Nogueira CW, Zeni G, et al. Physicochemical and biochemical profiling of diphenyl diselenide. Appl Biochem Biotechnol. 2013;169(3):885–893.
[16]   Sands KN, Tuck TA, Back TG. Cyclic seleninate esters, spirodioxyselenuranes and related compounds: new classes of biological antioxidants that emulate glutathione peroxidase. Chemistry. 2018;24(39):9714–9728.
[17]   Kipper AI, Titova AV, Borovikova LN, et al. Morphological characteristics of selenium–polyethyleneglycol nanocomposites. Russ J Phys Chem. 2015;89(9):1625–1627.
[18]   Luan J, Shen W, Chen C, et al. Selenium-containing thermogel for controlled drug delivery by coordination competition. RSC Adv. 2015;5(119):97975–97981.
[19]   Liu Y, Li B, Li L, et al. Synthesis of organoselenium-modified-cyclodextrins possessing a 1,2-benzisoselenazol-3(2H)-one moiety and their enzyme-mimic study. HCA. 2002; 85(1):9–18.
[20]   Li T, Smet M, Dehaen W, et al. Selenium–platinum coordination dendrimers with controlled anti-cancer activity. ACS Appl Mater Interfaces. 2016;8(6):3609–3614.
[21]   Tekade RK, Kumar PV, Jain NK. Dendrimers in oncology: an expanding horizon. Chem Rev. 2009;109(1):49–87.
[22]   Ooya T, Lee J, Park K. Hydrotropic dendrimers of generations 4 and 5: synthesis, characterization, and hydrotropic solubilization of paclitaxel. Bioconjug Chem. 2004;15(6): 1221–1229.

[23] Mohammadifar E, Kharat AN, Adeli M. Polyamidoamine and polyglycerol; their linear, dendritic and linear–dendritic architectures as anticancer drug delivery systems. J Mater Chem B. 2015;3(19):3896–3921.

[24] Mugabe C, Raven PA, Fazli L, et al. Tissue uptake of docetaxel loaded hydrophobically derivatized hyperbranched polyglycerols and their effects on the morphology of the bladder urothelium. Biomaterials. 2012;33(2):692–703.

[25] Mugabe C, Liggins RT, Guan D, et al. Development and in vitro characterization of paclitaxel and docetaxel loaded into hydrophobically derivatized hyperbranched polyglycerols. Int J Pharm. 2011;404(1–2):238–249.

[26] Cherri M, Ferraro M, Mohammadifar E, et al. Biodegradable dendritic polyglycerol sulfate for the delivery and tumor accumulation of cytostatic anticancer drugs. ACS Biomater Sci Eng. 2021.

[27] Braatz D, Dimde M, Ma G, et al. A tool box of biodegradable dendritic (poly glycerol sulphate)-SS-poly(ester) micelles for cancer treatment: stability, drug release and tumor targeting. Biomacromolecules. 2021;22(6):2625–2640.

[28] Richter A, Wiedekind A, Krause M, et al. Non-ionic dendritic glycerol-based amphiphilies: novel excipients for the solubilisation of poorly water-soluble anticancer drug sagopilone. Eur J Oharm Sci. 2010;40(1):48–55.

[29] Chintala S, Toth K, Cao S, et al. Se-methylselenocysteine sensitizes hypoxic tumor cells to irinotecan by targeting hypoxia-inducible factor 1alpha. Cancer Chemother Pharmacol. 2010;66(5):899–911.

[30] Yeo J-K, Cha S-D, Cho C-H, et al. Se-methylselenocysteine induces apoptosis through caspase activation and Bax cleavage mediated by calpain in SKOV-3 ovarian cancer cells. Cancer Lett. 2002;182(1):83–92.

[31] Aupérin A. Epidemiology of head and neck cancers: an update. Curr Opin Oncol. 2020;32(3):178–186.

[32] Lafin JT, Sarsour EH, Kalen AL. Methylseleninic acid induces lipid peroxidation and radiation sensitivity in head and neck cancer cells. Int J Mol Sci. 2019;20:1–15.

[33] Fernandes EGR, de Queiroz AAA, Abraham GA, et al. Antithrombogenic properties of bioconjugate streptokinase-polyglycerol dendrimers. J Mater Sci Mater Med. 2006;17(2):105–111.

[34] Duncan R, Izzo L. Dendrimer biocompatibility and toxicity. Adv Drug Deliv Rev. 2005;57(15):2215–2237.

[35] Silva AO, Queiroz AAA. 2012. Molecular dynamics simulations of polyglycerol dendrimers as carriers for haloperidol: theoretical and experimental results. COLAOB. [cited 2018 July 21]. Available from: www.metallum.com.br/7colaob/resumos/trabalhos_completos/12-009.docx.

[36] Higa OZ, Faria HAM, De Queiroz AAA. Polyglycerol dendrimers immobilized on radiation grafted poly-HEMA hydrogels: surface chemistry characterization and cell adhesion. Radiat Phys Chem. 2014;98:118–123.

[37] Santos PP, da Silva Nunes A, De Queiroz AAAE, et al. Interactions of polyglycerol dendrimers with human serum albumin: insights from fluorescence spectroscopy and computational modeling analysis. J Biomater Sci: Polym Edn. 2019;30:1–16.

[38] Haag R, Sunder A, Hebel A, et al. Dendritic aliphatic polyethers as high-loading soluble supports for carbonyl compounds and parallel membrane separation techniques. J Comb Chem. 2002;4(2):112–119.

[39] Sureshbabu VV, Narendra N. Protection reactions. In: Hughes AB, editor. Amino acids, peptides and proteins in organic chemistry: Volume 4: Protection reactions, medicinal chemistry, combinatorial synthesis. New York (EUA): Wiley-VCH Verlag GmbH & Co; 2011. p. 1–96.

[40] Bartoli G, Marcantoni E, Marcolini M, et al. Applications of CeCl(3) as an environmental friendly promoter in organic chemistry. Chem Rev. 2010;110(10):6104–6143.

[41] López-Soria JM, Pérez SJ, Hernández JN, et al. A practical, catalytic and selective deprotection of a Boc group in N,N'-diprotected amines using iron(III)-catalysis. RSC Adv. 2015;5(9):6647–6651.

[42] Comer J, Tam K. Lipophilicity profiles: theory and measurement. In Testa B, van de Waterbed H, Folkers G, Guy R, Comer J, Tam K, editors. Pharmacokinetic optimization in drug research: biological, physicochemical, and computational strategies. Weinheim: Wiley-VCH; 2001. p. 275–304.

[43] Ulusoy HI. Simple and useful method for determination of inorganic selenium species in real samples based on UV–VIS spectroscopy in a micellar medium. Anal Methods. 2015;7(3):953–960.

[44] Tominaga H, Ishiyama M, Ohseto F, et al. A water-soluble tetrazolium salt useful for colorimetric cell viability assay. Anal Commun. 1999;36(2):47–50.

[45] Gherghi IC, Girousi ST, Voulgaropoulos AN, et al. Study of interactions between DNA–ethidium bromide (EB) and DNA–acridine orange (AO), in solution, using hanging mercury drop electrode (HMDE). Talanta. 2003;61(2):103–112.

[46] Carnahan MA, Grinstaff MW. Synthesis and characterization of poly(glycerol-succinic acid) dendrimers. Macromolecules. 2001;34(22):7648–7655.

[47] Ibrahim ZT, Khammas ZAA, Al-Adilee KJ. Spectrophotometric and thermodynamic study for separation and preconcentration of trace amounts of selenium species after CPE. J Phys: Conf Ser. 2020;1664:012075.

[48] Kim R. Recent advances in understanding the cell death pathways activated by anticancer therapy. Cancer. 2005;103(8):1551–1560.

[49] Zheng S, Li X, Zhang Y, et al. PEG-nanolized ultrasmall selenium nanoparticles overcome drug resistance in hepatocellular carcinoma HepG2 cells through induction of mitochondria dysfunction. Int J Nanomed. 2012;7:3939–3949.

[50] An W, Lai H, Zhang Y. Apoptotic pathway as the therapeutic target for anticancer traditional Chinese medicines. Front Pharmacol. 2019;10:1–25.